Received 31 October 2023; accepted 18 November 2023. Date of publication 30 November 2023; date of current version 18 December 2023.

Digital Object Identifier 10.1109/OJCOMS.2023.3337004

Understanding the Limits of LoRa Direct-to-Satellite: The Doppler Perspectives

MUHAMMAD ASAD ULLAH [1,2] (Student Member, IEEE), GIANNI PASOLINI [3,4] (Member, IEEE), KONSTANTIN MIKHAYLOV [1] (Senior Member, IEEE), AND HIRLEY ALVES [1] (Member, IEEE)

[1]Centre for Wireless Communications, The University of Oulu, 90014 Oulu, Finland
[2]VTT Technical Research Centre of Finland Ltd., 90570 Oulu, Finland
[3]Department of Electrical, Electronic, and Information Engineering, University of Bologna, 40136 Bologna, Italy
[4]CNIT, University of Bologna, 40136 Bologna, Italy

CORRESPONDING AUTHOR: M. ASAD ULLAH (e-mail: Muhammad.AsadUllah@oulu.fi)

This work was supported in part by the Research Council of Finland (former Academy of Finland) 6G Flagship Programme under Grant 346208; in part by COST Action CA20120 INTERACT; and in part by Walter Ahlström Foundation. The work of Muhammad Asad Ullah was supported in part by Drolo, a project funded by Business Finland and the participating companies. The work of Konstantin Mikhaylov was supported by the Research Council of Finland (former Academy of Finland) MRAT-SafeDrone Project under Grant 341111.

ABSTRACT The Long Range (LoRa) modulation enables low-cost and low-power communications, serving as the foundation for the widely adopted terrestrial low-power wide-area network (LPWAN) technology known as LoRaWAN. Owing to its effectiveness, this modulation scheme is emerging as a potential option to provide direct-to-satellite (DtS) connectivity supporting Internet-of-Things (IoT) applications in remote or hard-to-reach areas, and complementing existing terrestrial networks. Besides the link budget and interference, the Doppler effect is one of the main challenges in LoRa DtS connectivity. Earlier studies have extensively investigated the link budget and the network scalability aspects, confirming the feasibility of integrating LoRa with Low Earth Orbit (LEO) satellites. However, only a few studies examine the influence of the Doppler effect on LoRa DtS performance. Specifically, the majority of the available literature report empirical studies that analyze the Doppler effect solely for a specific set of communication parameters. There remains a need for extensive and comprehensive examination of LoRa DtS performance under a strong Doppler effect in the LEO scenario. In this paper, we discuss and thoroughly investigate the impact of the Doppler effect on the reliability of LoRa satellite links. In particular, we analytically study packet losses, distinguishing the effect of Doppler shift from Doppler rate, the latter being caused by the variation in the relative speed of LEO satellites with respect to a terrestrial IoT end-device. Our analysis accounts for the effects of key communications parameters and settings, such as bandwidths, carrier frequency, MAC payload, LEO satellite's orbital height, and LoRaWAN low data rate optimization (LDRO). Notably, the results identify the LoRa boundaries for direct to LEO satellite connectivity and can facilitate the selection of suitable parameters for future system designs. Specifically, our results demonstrate that the packet delivery ratio of the most vulnerable spreading factor, i.e., SF12, exceeds 82% when using 125 kHz bandwidth, 433 MHz carrier frequency, and 59 bytes payload for a satellite orbiting at 560 km height.

INDEX TERMS Doppler effect, direct-to-satellite, LoRa, LoRaWAN, LPWAN, IoT, LEO, LDRO, orbit, satellite.

I. INTRODUCTION

WIRELESS communication is the cardiovascular system of modern society. Unfortunately, only 10% of Earth's surface is covered by terrestrial communication networks due to geographical, economic, and practical limitations. In fact, remote areas are generally characterised by poor or absent communication infrastructures, which hinder the provision of IoT services. To tackle this issue, massive Machine-Type Communication (mMTC) LPWAN technologies have been introduced in recent years [1],

supporting long-range communications. Taking it a step further, the concepts of non-terrestrial networks (NTNs) and non-terrestrial mMTC have been proposed to enable global connectivity for IoT applications [2], [3]. Industry and academia are thus focusing on the integration of mMTC and satellite communications to enable direct-to-satellite (DtS) global connectivity. This makes DtS a key component of the upcoming 6G communications networks. In fact, it is expected that products and services based on the DtS-IoT concept can contribute to achieving the United Nations Sustainable Development Goals. These expectations are supported by statistics, which reveal that there will be around 30.3 million satellite IoT devices deployed globally, and the related global market will exceed six billion dollars by 2025 [4]. The number of active satellites is expected to grow from 6,700 to 100,000 by 2030, offering support to novel IoT applications such as wildlife, smart agriculture, offshore wind farm as well as ship monitoring.

Under the MTC LPWAN umbrella, LoRaWAN is one of the most important and widely used protocols for establishing long-range communications. This makes LoRaWAN, which is based on the LoRa physical layer patented by Semtech [5], a prospective choice to enable satellite-based mMTC networks providing low-cost global coverage [6]. In this regard, the recent literature focuses extensively on link budget and interference analyses and confirms the feasibility of DtS communications between LoRaWAN devices and LEO satellites [6], [7], [8].

As is well known, in order to avoid falling back to Earth due to gravitational attraction, LEO satellites orbit at a speed much faster than the Earth's rotational speed. As a consequence of the relative motion of the satellite and the terrestrial end-devices, the transmitted signal's carrier frequency undergoes a significant change known as Doppler shift, whose magnitude varies over time during the satellite's visibility interval. The Doppler rate accounts for the speed of these variations and is calculated as the rate of change of the Doppler shift over time. Unfortunately, this phenomenon poses serious challenges to the physical layer of LoRa receivers [2], [3].

Focusing on this aspect, we realised that most previous studies present just the experimental results, which were obtained by considering only a limited subset of the parameters that affect the sensitivity of LoRa to the Doppler effect. Moreover, some critical settings (e.g., the orbital height) were fixed. Lastly, it's crucial to note that the majority of these studies, along with the currently operational LoRa satellites, are confined to communications within the 430 MHz band, which experiences the least impact from the Doppler effect among those allowed for LoRa signals. In this paper, we address this shortcoming by investigating all aspects affecting the robustness of LoRa DtS communications to the Doppler effect. The main contributions and novelty of this paper can be summarized as follows:

- First, we took as a reference the outcomes of flight-testing experiments [9], which were used to validate our approach, as well as Semtech documents [10], [11], [12], [13], [14], which were the basis to derive realistic results regarding the impact of the Doppler effect on LoRa DtS connectivity. Building upon these solid foundations, and differently from the existing literature, our analysis considers both the Doppler shift and the Doppler rate, quantifying the packet losses caused by each of them.
- Second, we assess the performance limits of the LoRa modulation under the influence of a strong Doppler effect caused by LEO satellite mobility, taking into account all communication parameters that affect the receiver's sensitivity to this phenomenon. Specifically, we consider the following parameters:
  1) MAC payload lengths;
  2) signal bandwidth;
  3) carrier frequency;
  4) spreading factor (SF);
  5) satellite orbital height.

  To the best of our knowledge, this is the first paper that theoretically assesses the impact of all these parameters on the robustness of LoRa to the Doppler effect. Importantly, this is the first paper ever to investigate the performance of LoRa DtS under strong Doppler effect in LEO scenario when operated in the S-band (2.1 GHz), a frequency range recently addressed by Semtech transceivers (LR1120) for direct communication with orbiting satellites.
- Third, we are the first to theoretically discuss the role of low data rate optimization (LDRO) feature, unveiling its operating principle and evaluating its impact on the robustness of LoRa receivers to the Doppler effect. Importantly, the effect of LDRO has not been discussed and investigated even for terrestrial LoRa connectivity. Hence, the findings presented on LDRO may prove valuable not only for NTNs but also for terrestrial networks.
- Fourth, we provide and discuss results that allow practitioners and researchers to select suitable settings to combat the Doppler phenomenon in LoRa DtS communications and ensure reliability. To facilitate the technical understanding of our framework and replication of our findings, we made the developed simulator openly accessible to the research community (available from GitHub via [15]).

The rest of this paper is organized as follows. Section II briefly presents the background of LoRa DtS systems and relevant studies. Section III briefly introduces the LoRa modulation focusing on the aspects related to Doppler and its effect on communication performance. Section IV suggests the system model to evaluate LoRa DtS performance in the presence of a Doppler effect. Selected numerical results are presented in Section V. In Section VI, key points and prospective directions for future research work are discussed. Finally, Section VII concludes this work with final remarks.

TABLE 1. Examples of launched LEO LoRa DtS systems [16].

Satellite	CubeSat	Quantity	Frequency	Purpose
Norby	6U	1	436.7 MHz	Research
FossaSat	2P*	13	401.7 MHz	Sat-IoT
Lacuna Sat	3U	5	868, 915 MHz	Sat-IoT
SATLLA-2B	2P	1	437.2 MHz	Research
FEES	0.3U	2	437.2 MHz	Experimental

* PocketQube

II. STATE-OF-THE-ART

A. LoRa DIRECT-TO-SATELLITE SYSTEMS

Recent experiments have confirmed the feasibility of direct communications from a LoRa end-device to a LEO satellite [9].

To provide concrete examples, Lacuna Space has launched five LEO satellites featuring a LoRa gateway onboard and confirmed the feasibility of receiving LoRa messages [8]. These satellites comply with ITU regional regulations and work on ISM radio bands 868 MHz (Europe) and 915 MHz (North America).

Similarly, more than 20 active LEO satellites feature LoRa modulation, including Norby, FOSSA, FEES, and SATLLA-2B. These satellites broadcast LoRa packets and more than five and half million LoRa packets have been successfully received by thousands of ground gateways as of October 2023 [16]. Table 1 provides the details of the above-mentioned trials, including the satellites' dimensions and purpose. It is worth noting that the 863-870 MHz band is not highly regarded due to its greater sensitivity to the Doppler effect compared to the band around 400 MHz. However, this band is of utmost importance as it provides coverage in many regions of the world and is close to the 902-928 MHz band, which offers coverage in the United States and Asia. In fact, dual-band 863-870 MHz and 902-928 MHz transceivers, which can be easily implemented due to the closeness of the two bands, would provide coverage in most regions of the world. This further motivates a comprehensive investigation into LoRa DtS performance in these bands, which is currently lacking in the existing literature.

B. RELEVANT WORKS

1) LINK BUDGET AND SCALABILITY PERSPECTIVE

In recent years, several studies have thoroughly explored the LoRa DtS communication link budget and scalability, taking into account various channel conditions and user densities, which reflect real-world application scenarios [7], [8], [17], [18], [19], [20]. Specifically, the work in [7] discusses various network configuration options and their respective pros and cons in order to facilitate the implementation of LoRa DtS. In [8], simulation results reveal that a radio packet featuring LoRa modulation could reach a LEO satellite even at a link distance of around 2300 km with more than 97% probability and the network can support massive connectivity. However, simultaneous transmissions from other end-devices cause same-channel interference and lower the packet delivery ratio [7], [8], [20]. Notably, advanced MAC protocols, compression, data aggregation, coding, scheduling, and time diversity can effectively mitigate packet losses due to interference. As of today, the number of studies investigating the impact of the Doppler effect on LoRa performance remains limited, both for terrestrial and non-terrestrial networks.

2) DOPPLER ASPECTS IN TERRESTRIAL NETWORKS

Extensive outdoor and laboratory experiments have been carried out on-ground using both a vehicle and a lathe machine to study the LoRa robustness against the Doppler effect [21]. The obtained results highlight that the higher SFs (e.g., SF=12) are more vulnerable to Doppler shift than the lower SFs in the mobile scenario. In [22], authors evaluate the performance of LoRa in six typical terrestrial V2X communications scenarios. These scenarios account for varying vehicle velocities ranging from 32 to 104 kmph, resulting in Doppler shifts between 300 and 400 Hz. Monte Carlo simulations were employed to analyze the impact of the Doppler shift on communication performance. The results indicate a degradation in the LoRa communication performance due to the Doppler shift.

3) DOPPLER ASPECTS IN NON-TERRESTRIAL NETWORKS

Compared with terrestrial vehicles, LEO satellites cause a much larger Doppler shift by orbiting Earth at an average speed in the order of thousands of kilometers per hour (e.g., 27,000 kmph for an orbital height of 780 km [7]). Only a few studies assess the LoRa robustness against the Doppler effect in LEO satellite scenario. In [23], the first study was presented that aimed at evaluating the impact of the Doppler effect on the LoRa modulation in an attempt to understand the stability of LoRa DtS communications. Specifically, laboratory experiments were conducted to test the LoRa modulation with a carrier frequency of 430 MHz and a CubeSat orbiting at 200 km. The work was further extended in [6], where the authors report the results of laboratory and outdoor experiments. A radio frequency (RF) vector signal generator and a LoRa end-device based on the Semtech SX1278 transceiver were used as transmitter and receiver, respectively. Considering a carrier frequency of 434 MHz, the vector generator was used to synthesize LoRa signals to account for Doppler shifts corresponding to 200 km and 550 km orbital heights.

Following the laboratory and outdoor tests, the authors of [6], [23] launched a Norby–CubeSat with an on-board SX1278 transceiver, which orbits at 560 km and operates at 436.7 MHz [24]. In [9], the first flight-testing experiments are described, establishing the foundation for understanding the LoRa modulation's capabilities and constraints at 436.7 MHz. Specifically, 20 experiments were carried out to examine the LoRa robustness against the Doppler effect for different SFs, bandwidths and payload (P_L) size. Similar

TABLE 2. The list of the works investigating the LoRa DtS performance under Doppler effect, their methodology and the set of parameters they account for. The references are I [23], II [6], III [9], IV [25] and V [26].

Parameters	I	II	III	IV	V	Our work
SF	7, 11	7,8,11,12	7,10,11,12	7-12	7-12	7,10,12
B **(kHz)**	125 250	62.5, 125 125, 500	31.25, 62.5 125, 500	125	- -	31.25, 62.5 250, 500
P_L **(bytes)**	255	21,59 255	55 143	64,128 235	12	1-59 255
F_C **(MHz)**	430	434	436.7	868	866.3	433,436.7,868,2100
LDRO	enabled	enabled disabled	enabled	- -	- -	enabled disabled
H **(km)**	200	200 550	560	200 550	650	560-1500
Empirical	✓	✓	✓	✓	×	×
Open source	×	×	×	×	×	✓

to results in [6], [23], the flight-testing experiments confirm LoRa's strong immunity to the Doppler effect when using $7 \leq SF \leq 11$ and bandwidth $B > 31.25$ kHz. These experiments[1] assess the LoRa DtS performance accounting for both the Doppler shift and the Doppler rate, and key findings are:

- the Doppler shift, also called static Doppler, degrades the communication performance at the lowest elevation angles and the maximum link distance;
- the Doppler rate, also referred to as dynamic Doppler, causes packet losses at high elevation angles, when the satellite is positioned just above the end-device on the ground, resulting in the closest link distance.

Specifically, at low elevation angles, communication experiences a maximum Doppler shift. Consequently, the carrier frequency of the received signal deviates significantly from the carrier frequency of the transmitted signal. This discrepancy may lead to the failure of the Phase-Locked Loop (PLL) at the receiver's side to track the incoming signal, resulting in packet loss. Conversely, the Doppler rate, characterizes change of carrier with time from its initial value, can impact the receiver's ability to remain locked onto the received carrier. As an example, as discussed in [6], [9], [23], at a 90 degree elevation angle, the Doppler shift is as low as 0 kHz, posing no issues to the PLL. However, at the same 90 degree elevation, there is a very high Doppler rate, such as nearly –270 Hz/s for 868 MHz with a satellite orbiting at 550 km. Despite the PLL's ability to lock onto the signal at this angle, it may fail to remain locked due to the high Doppler rate. To visually convey this issue, Figure 1 illustrates the region affected by the Doppler shift (marked in gray) and the Doppler rate (indicated in red).

More recently, an experiment was presented in [25], where a software-defined radio (SDR) was used to emulate the Doppler effect in a LoRa satellite link at 868 MHz for a limited set of communication parameters. Consistent with the findings in [6], [9], [23], the results lead to the conclusion that LoRa DtS links are more impacted by the Doppler rate than the Doppler shift.

1. For the sake of completeness, the experiment configuration in the reported works was: transmission power 4 W, two packet sizes (55 bytes and 143 bytes), and SF7, SF10, SF11 and SF12.

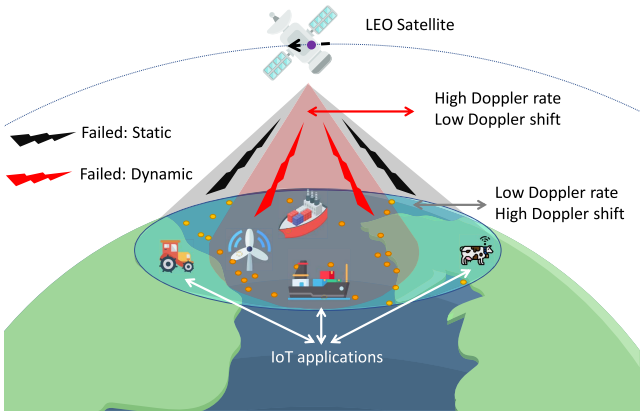

FIGURE 1. Illustration of the communication failure due to Doppler shift (failed: static) and Doppler Rate (failed: dynamic) in DtS IoT scenario.

The authors of [26] propose a receiver architecture to counteract the Doppler phenomenon, while a regression-based pilot is designed in [27] for Doppler shift estimation and compensation at the receiver end.

As shown in Table 2, these previous studies mostly report experimental results for a fixed and limited subset of parameters and lack an analytical framework to generalize the investigation on the Doppler effect. Specifically, the findings in papers I [23], II [6], III [9] and IV [25] of Table 2, are rooted in empirical testing, making it challenging to replicate, reproduce and generalize the results outlined in these works. Conversely, the work in V [26] adopts a theoretical approach, focusing on the analysis of LoRa performance within a LEO scenario, but for a predefined set of parameters without offering information about bandwidth and LDRO. Furthermore, the majority of these studies concentrate on the band around 430 MHz, which experiences

the least impact from the Doppler effect among those allowed for LoRa signals. Unlike the works in I-V, we also study the LoRa DtS performance for the 2.1 GHz channel (note that the newly introduced LoRa LR1120 modems intends to support 2.1 GHz band). More than this, in the present paper, we do extensive analysis accounting for a range of communication and orbital parameters to identify the limits of LoRa in LEO. Additionally, we provide an openly accessible framework that empowers readers to replicate and extend our results (available from GitHub via [15]).

III. LoRa MODULATION

To better understand the impact of the Doppler effect on LoRa DtS links, we briefly revise the key points on the LoRa modulation, which is derivative of the chirp spread-spectrum (CSS) modulation. As is well known, a sine-wave chirp signal, concisely denoted "chirp" in the following, consists of a sinusoid whose frequency linearly sweeps within a given interval B. With reference to LoRa, in particular, having denoted with

- $\mathrm{SF} \in \{7, 8, 9, 10, 11, 12\}$, the spreading factor,
- $B \in \{31.25, 62.5, 125, 250, 500\}$ kHz, the bandwidth,
- $M = 2^{\mathrm{SF}}$, the cardinality of the modulation alphabet,
- T_c the chirp duration, chosen such that $BT_c = M$,

it is observed that, for a given SF, the LoRa transmitter has at its disposal a set of $M = 2^{\mathrm{SF}}$ different chirps, each of which is in one-to-one correspondence with one of the M symbols of the modulation alphabet $\mathcal{S} = \{0, 1, 2, \ldots, M-1\}$. It follows that, given the adopted SF, for each sequence of SF data bits to be transmitted, the modulator selects the corresponding modulation symbol within $\mathcal{S}$ and transmits the chirp with which that symbol is uniquely associated.

It is worth emphasizing that the M chirps are different in that they start sweeping from different initial frequencies, which are regularly spaced with a frequency step $\Delta f = \frac{B}{M}$ Hz [5]. This means that larger SFs, which correspond to lower values of Δf, are more sensitive to the Doppler effect because of the lower frequency separation between chirps.

To increase the robustness to Doppler rate, LoRa features the LDRO mode, which reduces by two the number of bits carried by each symbol. This means that, for a given SF, the cardinality of the modulation alphabet reduces to $M = 2^{(\mathrm{SF}-2)}$, as does the number of chirps packed in the bandwidth B, which entails that the LDRO mode increases the frequency separation Δf between chirps by four times and, therefore, the resistance to Doppler rate. Clearly, this positive result comes at the cost of reducing the data rate.

IV. SYSTEM MODEL

In this section, we discuss the analytical framework used for investigating the performance of the LoRa modulation when subjected to a strong Doppler effect in LEO DtS links. Unless otherwise specified, we consider the most widespread DtS IoT scenario, where a terrestrial IoT end-device transmits a signal to a satellite-based LoRaWAN gateway [7], [8], [20].

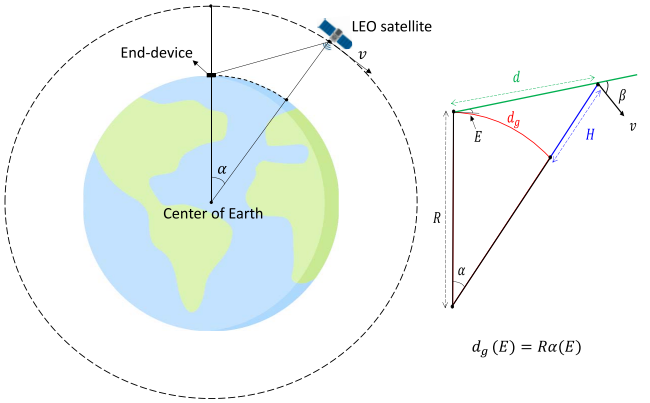

FIGURE 2. The satellite ↔ end-device (ground terminal) basic geometry.

However, the suggested framework remains valid and can be easily modified to account for the opposite scenario, wherein the satellite acts as a transmitter, and a terrestrial end-device serves as the receiver.

A. SATELLITE AND END-DEVICE GEOMETRY

To investigate the LoRa DtS performance, it is fundamental to understand the satellite↔end-device geometry depicted in Figure 2. First, the mobility of the LEO satellite rapidly changes the elevation angle E, resulting in variations of the slant distance d. Based on the geometric relations shown in Figure 2, one can find d from a given E and vice versa as [8]

$$d(E) = R\left[\sqrt{\left(\frac{H+R}{R}\right)^2 - \cos^2(E)} - \sin(E)\right] \tag{1}$$

$$E(d) = \sin^{-1}\left(\frac{H^2 + 2HR - d^2}{2dR}\right) \tag{2}$$

where $R = 6371$ km is radius of Earth, H is the orbital height of the satellite and E is expressed in degrees.[2] The projection on the Earth's surface of the segment connecting the end-device and the satellite creates an arc defined as ground range $d_g(E)$. The length of the arc is equivalent to the product of Earth's radius R and the central angle $\alpha(E)$ as [28], [29]

$$d_g(E) = R\alpha(E) = R\sin^{-1}\left(\frac{d(E)\cos(E)}{R+H}\right) \tag{3}$$

where α is in radians.

For a given H, the maximum satellite visibility time τ depends on $d_g(E_{\min})$. We imply $E_{\min}$ is the minimum elevation angle, which, in the most simple case, will be equal to 1 degree. Following the satellite orbital velocity and ground range relation, the total visibility time is defined by

$$\tau = 2\frac{d_g(E_{\min})}{v} \tag{4}$$

2. On the left-hand side of eqs. (1) and (2) we emphasized only the dependence on E, because R and H are constant.

where v is the velocity of the satellite in the circular orbit and can be computed by $v = \sqrt{\frac{g \cdot R}{1+\frac{H}{R}}}$, where g is gravitational acceleration on the Earth [6].

B. DOPPLER SHIFT AND DOPPLER RATE

To maintain the circular orbit, LEO satellites revolve around the Earth at very high speed, which results in a relative motion of the satellite relative to a stationary observer/end-device on the Earth's surface. Unfortunately, this phenomenon introduces a significant frequency shift in the received radio signal, hindering proper demodulation. Specifically, at a given instant of time (t), the difference between the transmitted carrier frequency F_C and the received carrier frequency $F_R(t)$, the latter varying in time owing to the satellite motion, is known as Doppler shift, given by

$$F_D(t) = F_R(t) - F_C, \tag{5}$$

whereas its derivative

$$\Delta F_D(t) = \frac{d(F_D(t))}{dt} \tag{6}$$

is called the Doppler rate.

Given the geometry depicted in Figure 2, the mathematical expression of $F_R(t)$ as a function of F_C is given by [6]

$$F_R(t) = \frac{1}{1 + \frac{v}{c}\cos(\beta(t))} F_C \tag{7}$$

with

$$\cos(\beta(t)) = \frac{\sin(\varphi(t))}{\sqrt{\left(1+\frac{H}{R}\right)^2 - 2\left(1+\frac{H}{R}\right)\cos(\varphi(t)) + 1}} \tag{8}$$

where β is the angle between the satellite velocity vector and the direction to the terrestrial end-device [6] and $\varphi(t)$ is expressed as

$$\varphi(t) = t\sqrt{\frac{g}{R}}\left(1+\frac{H}{R}\right)^{-3/2}, \tag{9}$$

being $-\frac{\tau}{2} \leq t \leq \frac{\tau}{2}$ the relative elapsed time. Note that $t = 0$ corresponds to a satellite being at $E = 90°$ and having minimum slant distance d to the observer/end-device.

In the following, we will distinguish between the static Doppler, which refers to the Doppler shift experienced by the receiver at the beginning of packet reception, and the dynamic Doppler, which represents the additional, time-varying, frequency shift that occurs throughout the packet reception interval. The former pertains to the receiver's ability to lock onto the received carrier frequency when an incoming packet is detected (i.e., at the beginning of the packet reception). The latter, instead, is related to the receiver's ability to remain locked onto the received carrier despite its deviations over time from the initial value.

Let us clarify that the need to explicitly introduce the two components of the Doppler shift, namely the static Doppler and the dynamic Doppler, into our analytical framework arises from the fact that Semtech documents [12], [13], [14] on the LoRa modulation provide the requirements for robust demodulation against these two contributions separately. This aspect will be discussed in the following section.

TABLE 3. LoRa intra-packet dynamic Doppler shift limits ($F_{dynamic}$) in Hz.

	LDRO Disabled		LDRO Enabled	
SFs	**125 kHz**	**500 kHz**	**125 kHz**	**500 kHz**
SF7	325.5	1302.1	5208.3	20833.3
SF8	162.8	651	2604.2	10416.7
SF9	81.4	325.5	1302.1	5208.3
SF10	40.7	162.8	651	2604.2
SF11	–	81.4	325.5	1302.1
SF12	–	40.7	162.8	651

C. LoRa DOPPLER SHIFT TOLERANCE

According to experimental flight tests [9] and Semtech documents [10], [11], LoRa exhibits tolerance to a frequency offset of up to ±25% of the bandwidth B without any sensitivity degradation. Thus, the immunity limit for the static Doppler becomes

$$F_{static} = \pm 0.25 \times B. \tag{10}$$

At the same time, proper LoRa demodulation requires that the carrier frequency variation within the duration of the received packet, which is due to the experienced Doppler rate, does not exceed a given threshold. More precisely, the variation of the carrier frequency over the packet reception time (between the beginning and the end of the packet) should remain below [12], [13], [14][3]

$$F_{dynamic} = \frac{L \times B}{3 \times 2^{SF}} \tag{11}$$

where $L = 16$ when LDRO is enabled, otherwise, $L = 1$. In LoRaWAN, LDRO is recommended when the LoRa symbol duration exceeds 16.38 ms. With B=125 kHz, SF11 and SF12 have symbol time greater than 16.38 ms, consequently, LDRO is mandated by the LoRaWAN specification for these spreading factors. As already observed, due to the larger frequency separation between chirps, LDRO enhances the LoRa immunity to dynamic Doppler. In this regard, Table 3 shows the values of $F_{dynamic}$ calculated using (11) for different SFs and bandwidths B, with and without LDRO.

To model the effect of the Doppler effect on LoRa DtS performance, we suggest the following conditions to account for the packet loss due to (i) static Doppler; (ii) dynamic Doppler and (iii) joint static and dynamic Doppler.

Let $L_{static}(t) \in \{0, 1\}$ reflects a successful or lost packet due to Doppler shift, where:

$$L_{static}(t) = \begin{cases} 1 & \text{if } |F_D(t)| \geq |F_{static}| \\ 0 & \text{else} \end{cases} \tag{12}$$

3. Notably, in [12], [13], [14], Semtech does not provide any explanation for the formulation of equations (10) and (11).

Let $L_{\text{dynamic}}(t) \in \{0, 1\}$ reflects a successful or lost packet due to Doppler rate, where:

$$L_{\text{dynamic}}(t) = \begin{cases} 1 & \text{if } |\Delta F_E| \geq F_{\text{dynamic}} \\ 0 & \text{else} \end{cases} \tag{13}$$

with ΔF_E denoting the overall change in the carrier frequency from the beginning to the end of the packet, defined as

$$\Delta F_E = F_{\text{D}}[t_{\text{start}}] - F_{\text{D}}[t_{\text{end}}] \tag{14}$$

where t_{start} denotes the time instant at the beginning of the packet reception, and $t_{\text{end}} = t_{\text{start}} + \text{ToA}$ represents the time instant at the end of the packet reception.

The Time on Air (ToA) is given by $\text{ToA} = T_{\text{s}} \times N_{\text{s}}$, where $T_{\text{s}} = \frac{2^{\text{SF}}}{B}$ is the symbol duration, which is equal to the chirp duration T_{c}, and N_{s} is the number of symbols (that is, of chirps) in a packet (refer to [10] for further details.

Let $L_{\text{joint}}(t) = L_{\text{static}}(t) \times L_{\text{dynamic}}(t)$ be the packet loss due to joint Doppler shift and Doppler rate, where $L_{\text{joint}}(t)$ is 1 for lost packet and 0 otherwise. It is important to mention that we use $L_{\text{static}}(t)$, $L_{\text{dynamic}}(t)$, and $L_{\text{joint}}(t)$) in Algorithm 1, intending to help potential readers to understand how we have generated the results for our analysis. Algorithm 1 assess the performance during full satellite visibility time interval, i.e., $-\frac{\tau}{2} \leq t \leq \frac{\tau}{2}$; therefore, lines 9–27 represent a loop going through all possible time instances (t) and covering the entire range of elevation angles.

D. AVERAGE PACKET DELIVERY RATIO

The average Packet delivery ratio (PDR) is the ratio of successfully received packets over transmitted ones during the full visibility time τ of the satellite pass covering the full visibility interval $-\frac{\tau}{2} \leq t \leq \frac{\tau}{2}$.

Let us denote S_{loss}, D_{loss}, and J_{loss} as the number of lost packets due to static, dynamic, and joint Doppler shift, respectively. Thus, one can find PDR as

$$PDR = 1 - \frac{P_{\text{lost}}}{P_{\text{total}}} = 1 - \frac{S_{\text{loss}} + D_{\text{loss}} - J_{loss}}{P_{\text{total}}}, \tag{15}$$

where $P_{\text{total}} = \frac{\tau}{R_p}$, and R_p represents the average interval between the start of transmissions of two consecutive packets, assuming periodic reporting.

V. RESULTS

It is worth recalling that our analysis solely considers packet losses due to the Doppler effect, encompassing both the Doppler shift and the Doppler rate. We model a single end-device without co-channel interference, assuming no link budget constraint. This implies the signal is strong enough to reach a LEO satellite in orbit. Note that interference and link budget have been extensively studied in previous works, which confirmed the feasibility of LoRa DtS communication as discussed in Section II-B. For a comprehensive investigation on LoRa DtS communications, link budget and interference analyses can be added on top of the analysis presented in this paper, as demonstrated in [7], [8].

Algorithm 1 LoRa DtS Performance Under Doppler Effect for Entire Visibility Interval $-\frac{\tau}{2} \leq t \leq \frac{\tau}{2}$

1: **Input**: E, B, F_{C}, LDRO, SF, P_L, H
2: **Initialization:** $S_{\text{loss}} = 0$, $D_{\text{loss}} = 0$, $J_{\text{loss}} = 0$
3: **Constants:** $R = 6371$ km, $g = 9.80665$ m/s^2
4: $\tau \leftarrow$ satellite total visibility time calculated by (4)
5: ToA $\leftarrow$ LoRa Time on Air depends on P_L
6: $F_{\text{static}} \leftarrow$ Doppler shift tolerance threshold by (10)
7: $F_{\text{dynamic}} \leftarrow$ Doppler rate tolerance threshold by (11)
8: $t = -\frac{\tau}{2} \leftarrow$ Initialization of the interval
9: **while** $t \leq \frac{\tau}{2}$ **do**
10: $F_{\text{D}}(t) \leftarrow$ Doppler shift calculated by (5)
11: $\Delta F_{\text{D}}(t) \leftarrow$ Doppler rate calculated by (6)
12: $\Delta F_E(t) \leftarrow$ Total frequency change over the packet transmission calculated by (14)
13: $L_{\text{static}}(t) \leftarrow$ Packet status under Doppler shift calculated by (12)
14: $L_{\text{dynamic}}(t) \leftarrow$ Packet status under Doppler rate calculated by (13)
15: $L_{\text{joint}}(t) \leftarrow$ Packet status under joint Doppler shift and rate as $L_{\text{static}}(t) \times L_{\text{dynamic}}(t)$
16: **if** $L_{\text{static}}(t) == 1$ **then**
17: S_{loss}++; ▷ Packet fail due to Doppler shift
18: **end if**
19: **if** $L_{\text{dynamic}}(t) == 1$ **then**
20: D_{loss}++; ▷ Packet fail due to Doppler rate
21: **end if**
22: **if** $L_{\text{joint}}(t) == 1$ **then**
23:
24: J_{loss}++; ▷ Packet fail due to both Doppler shift and rate
25: **end if**
26: t++; ▷ Step increment of the time
27: **end while**
28: PDR $\leftarrow$ PDR calculated based on (15)
29: **Output:** PDR, $L_{\text{static}}(t)$, $L_{\text{dynamic}}(t)$, $L_{\text{joint}}(t)$

For our investigations, we used the analytical framework outlined in Section IV-B and the MATLAB Satellite Communications (SatCom) Toolbox, with the ultimate goal of modelling the Doppler effect experienced in the satellite communication links considered below.

Focusing the attention on the LoRaWAN frequency bands for Asia, Europe, and North America, Figure 3 shows the Doppler shift and Doppler rate for carrier frequencies F_{C} equal to 436.7 MHz, 868 MHz, and 2.1 GHz, with solid lines denoting Norby's two-line element (TLE),[4] corresponding to $H = 560$ km, and markers representing analytical results, respectively. In Figure 3 the simulation time $-\frac{\tau}{2} < t < \frac{\tau}{2}$ reported in the x-axis also accounts for the direction of satellite mobility, where τ is the satellite's total visibility time by a terrestrial user calculated by (4).

4. A TLE is a data format encoding a list of orbital elements of an Earth-orbiting object.

TABLE 4. Key communication parameters.

Parameters	Values
Bandwidth (B)	31.25, 62.5, 125, 250, 500 kHz
Carrier frequency (F_C)	433, 436.7, 868 MHz & 2.1 GHz
Spreading Factor (SF)	7, 10, 12
Code Rate	4/5
MAC Payload	1-59, 55, 250 bytes
LDRO	Enabled & Disabled
Orbital height	560-1500 km
Packet reporting period (R_p)	5 s

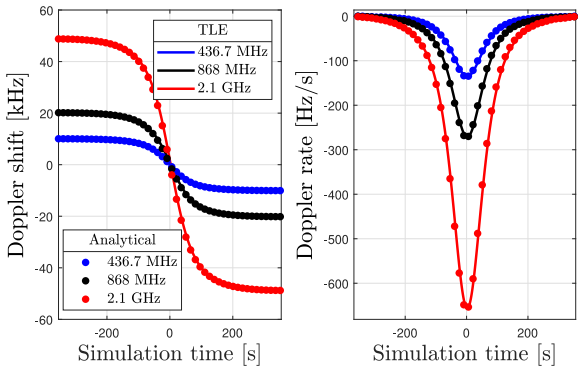

FIGURE 3. Comparison of the Doppler shift and Doppler rate generated from TLE and the analytical framework.

Specifically, the simulation time t considers the three possible scenarios as follows:

- $-\frac{\tau}{2} < t < 0$ account for the scenario when the satellite is moving toward the end-device. Following (7), $F_R(t)$ is higher than the carrier frequency F_C, resulting in a positive Doppler shift $F_D(t)$.
- when $t = 0$ the satellite is directly above the end-device ($E = 90°$), causing the Doppler shift $F_D(t) = 0$ kHz while the Doppler rate ΔF_D reaches its negative peak.
- $0 < t < \frac{\tau}{2}$ concerns the situation in which the satellite moves away from the end device, resulting in a negative Doppler shift $F_D(t)$.

One can see that the results obtained from MATLAB SatCom Toolbox match the Doppler model.

More than this, we use the SatCom toolbox with the Norby's TLE set to make a comparison with actual flight-tests [9]. Therefore, unless otherwise stated, we have considered $H = 560$ km as in [9] as well as $F_C = 436.7$ MHz, $B = 31.25$, 62.5, 125 kHz and $P_L = 55$ bytes. Starting from this baseline, we carried out our investigations by varying the orbital and communication settings. In particular, Table 4 lists the key communication parameters/orbital heights investigated in the current paper.

Following Algorithm 1, Figure 4 to Figure 7 show performance at a specific time instant t during the satellite visibility interval $-\frac{\tau}{2} < t < \frac{\tau}{2}$. The marker (dots) colour scheme is:

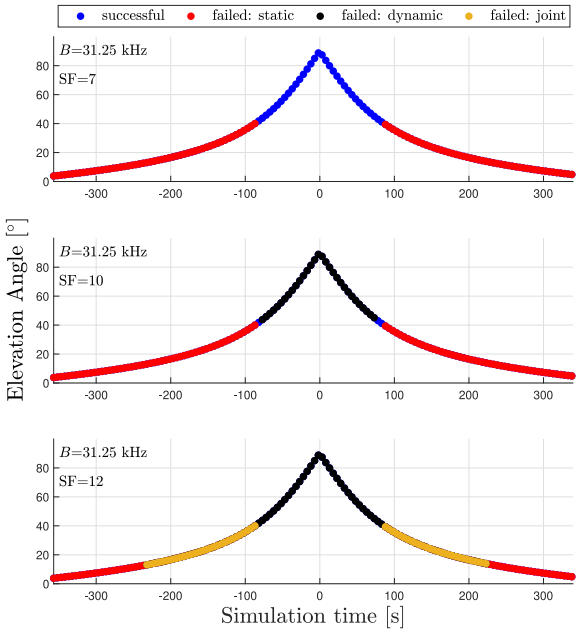

FIGURE 4. Impact of variable SFs on LDRO-enabled LoRa performance under Doppler effect at $B = 31.25$ kHz, $P_L = 55$ bytes, $F_C = 436.7$ MHz, and $H = 560$ km for SF = [7, 10, 12] with ToA = [595, 3285, 10517] ms, respectively.

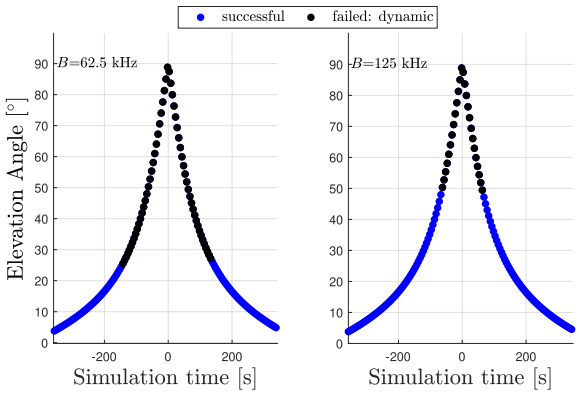

FIGURE 5. Impact of variable bandwidth ($B = 62.5$ kHz and 125 kHz) on LDRO-enabled LoRa performance under Doppler effect for $SF = 12$ at $P_L = 55$ bytes, ToA = [5259, 2629] ms, $F_C = 436.7$ MHz, and $H = 560$ km.

- Blue dots represent scenarios where $L_{static}(t) = 0$, $L_{dynamic}(t) = 0$, and $L_{joint}(t) = 0$ indicating no packet loss;
- A red dot indicates, $L_{static}(t) = 1$, $L_{dynamic}(t) = 0$, and $L_{joint}(t) = 0$, i.e., packet loss due to static Doppler;
- A black dot denotes that $L_{static}(t) = 0$, $L_{dynamic}(t) = 1$, and $L_{joint}(t) = 0$ showing the packet loss due to Dynamic Doppler;
- A yellow dot represents a scenario where $L_{static}(t) = 1$, $L_{dynamic}(t) = 1$ and $L_{joint}(t) = 1$, indicating packet loss due to both static and dynamic Doppler shifts.

Whereas Figure 8 to Figure 10 illustrate the average packet PDR across the entire range of elevation angles covering the complete satellite's visibility interval, i.e., $-\frac{\tau}{2} \leq t \leq \frac{\tau}{2}$. More

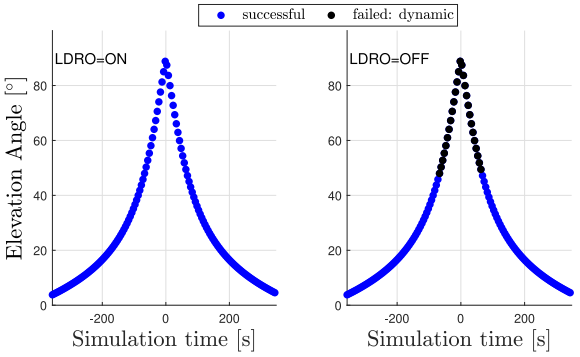

FIGURE 6. Impact of LDRO on LoRa performance for SF = 10 and $B = 125$ kHz, $F_C = 436.7$ MHz, $H = 560$ km with maximum allowed MAC payload $P_L = 59$ bytes.

than this, Figure 8 to Figure 10 also examine the standard LPWAN band 433 MHz.

A. BANDWIDTH

As (10) indicates, the LoRa modulation becomes more and more vulnerable to the static Doppler as the bandwidth B decreases. Considering $B = 31.25$ kHz and a payload length of 55 bytes, Figure 4 shows the correct (blue dot) or incorrect (black, red, and yellow dots) reception of packets for each time instant (x-axis) and corresponding elevation angle E (y-axis) during the satellite visibility interval. The colour code specified in the legend makes it possible to distinguish whether the failure is due to static Doppler, dynamic Doppler, or both, as dictated by (12) and (13).

One observes that, in the considered case, the static Doppler shift leads to packet loss for $E \leq 40°$, whatever SF is adopted. Differently from SF7, which performs well when $E > 40°$, SF10 and SF12 are irreparably affected by the dynamic Doppler (the change in frequency from the beginning to the end of packet reception) caused by the rate of change of Doppler shift. In fact, higher elevations lead to higher (in terms of absolute value) Doppler rates (see Fig. 3), which, together with the longer ToA due to higher SFs, cause the frequency deviation within the packet duration to exceed the threshold (11). In particular, SF10 appears vulnerable to the dynamic Doppler from $E > 40°$, while SF12 starts to suffer as early as $E > 13°$.

Better performance is instead expected for larger bandwidths. Indeed, increasing B raises F_{static}, thus improving the robustness of LoRa to the static Doppler, and reduces ToA, thus increasing its ability to combat the dynamic Doppler. Our analysis reveals that SF7 and SF10 have strong immunity to the Doppler effect when $B = 62.5$ kHz and $B = 125$ kHz, with correct packet reception in 100% of cases. However, as evident in Figure 5, SF12 remains vulnerable to the dynamic Doppler when $E > 24°$ and $E > 45°$ for $B = 62.5$ kHz and $B = 125$ kHz, respectively.

It is worth emphasizing the good match between the results shown in Figure 4 and the flight test results presented in [9] (Fig. 9, and Table 3), which confirms the validity of our methodology and the framework proposed.

TABLE 5. The range of elevation angles for successful operation for a satellite orbiting at $H = 560$ km, $P_L = 55$ bytes and LDRO-enabled mode.

F_C MHz	B kHz	SF7	SF10	SF12
436.7	31.25	$40° < E \leq 90°$	$40° < E < 43°$	-
	62.5	$\leq 90°$	$\leq 90°$	$< 25°$
	125	$\leq 90°$	$\leq 90°$	$< 50°$
868	31.25	$67° < E \leq 90°$	-	-
	62.5	$40° < E \leq 90°$	$40° < E < 64°$	-
	125	$\leq 90°$	$\leq 90°$	$< 35°$
2100	31.25	$77° < E \leq 90°$	-	-
	62.5	$70° < E \leq 90°$	-	-
	125	$50° < E \leq 90°$	$50° < E \leq 90°$	-

B. LOW DATA RATE OPTIMIZATION

Our analysis reveals that SF7 has a high tolerance to intra-packet frequency deviations, with and without LDRO. Specifically, when $B = 125$ kHz, SF7 supports a maximum MAC payload of 250 bytes, resulting in ToA = 548 ms. From Figure 3 one observes that when $F_C = 436.7$ MHz, the maximum Doppler rate is 144 Hz/s. Consequently, a 548 ms long SF7 packet will experience a dynamic Doppler shift of 78.9 Hz, far lower than the limits in Table 3.

On the other hand, by increasing SF, and consequently ToA, one expects less immunity to the dynamic Doppler. In fact, looking at Figure 6 we see that packet losses occur for an SF10 packet of 59 bytes (the maximum allowed length) when LDRO is disabled and $E \geq 47°$. Interestingly, no packet loss is observed when LDRO is enabled.

C. CARRIER FREQUENCY

The role played by the carrier frequency is investigated in Figure 7, in the case $B = 125$ kHz and $P_L = 55$ bytes for SF = [7, 10, 12] with ToA = [149, 821, 2629] ms. One observes that, despite the high Doppler effect at 868 MHz, SF7 and SF10 (and therefore also the intermediate SFs) show high stability without any losses, whereas SF12 suffer from dynamic Doppler (owing to the increased ToA) when $E \geq 35°$. However, significant packet losses occur by increasing the carrier frequency to 2.1 GHz. Specifically, SF7 and SF10 packets are lost when $E \leq 50°$ due to the static Doppler, whereas SF12 always fails to deliver packets due to static, dynamic, and joint Doppler shifts.

A comprehensive overview is provided in Table 5, presenting the elevation angle (E) ranges for successful LoRa DtS communications. The table outlines the specific spreading factors (SFs) along with carrier frequency and bandwidth combinations.

In the case $F_C = 436.7$ MHz, a bandwidth of 31.25 kHz allows a success range $40° < E \leq 90°$ for SF7, while for SF10, the success range narrows to $40° < E < 43°$. For SF12, the communication fails for the entire range of the E. For wider bandwidths of 62.5 kHz and 125 kHz, the results remain similar for SF7 and SF10, with successful operations over the entire range of the E. On the other hand, LoRa DtS featuring SF12 is only feasible when $E < 25°$, if $B = 62.5$ kHz, and $E < 50°$, if $B = 125$ kHz. This is due to

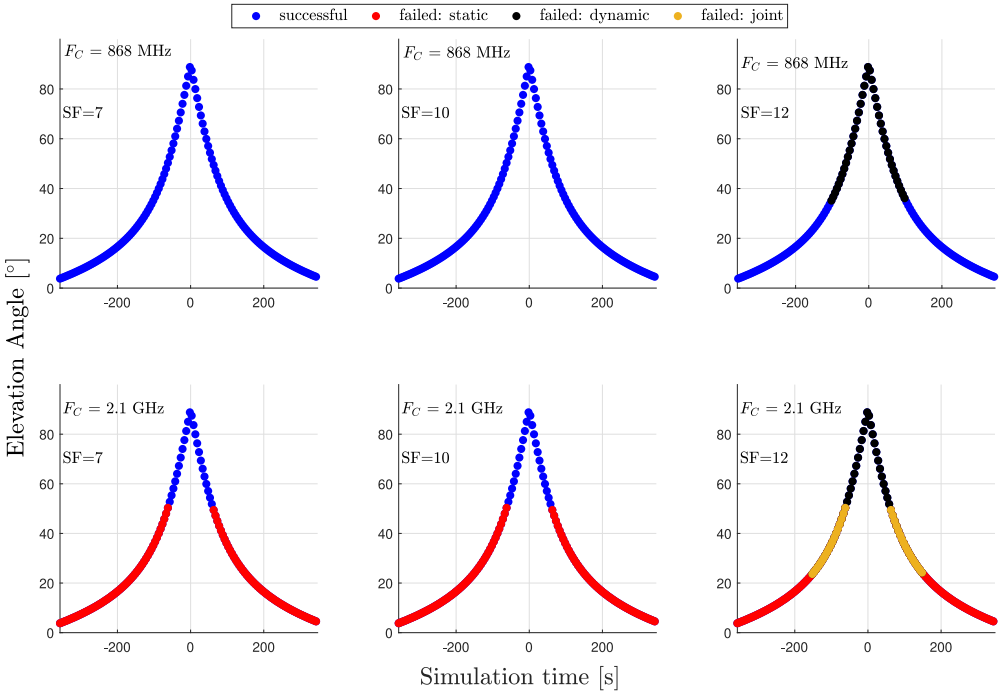

FIGURE 7. Impact of high carrier frequency on LDRO-enabled LoRa performance for $B = 125$ kHz, $H = 560$ km and $P_L = 55$ bytes for SF = [7, 10, 12] with ToA = [149, 821, 2629] ms, respectively.

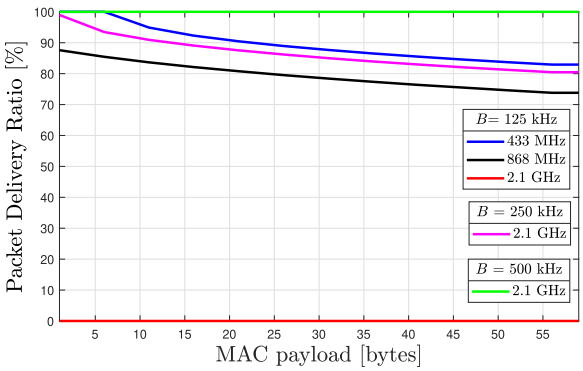

FIGURE 8. Impact of variable MAC payload on SF12 PDR at $B = 125$ kHz, 250 kHz, and 500 kHz, $F_C = 433$ MHz, 868 MHz and 2.1 GHz for a LEO satellite orbiting at $H = 560$ km.

the fact that SF12 features the higher ToA, which makes it more vulnerable to Doppler Rate resulting in packet losses.

At 868 MHz, when $B = 31.25$ kHz successful communication is limited to SF7 within the range $67° < E \leq 90°$. Conversely, SF10 and SF12 experience failure across the entire range of elevation angles due to both Doppler shift and Doppler rate. With a $B = 62.5$ kHz, SF7 offers connectivity within the range $40° < E \leq 90°$, while SF10's success range extends to $40° < E < 64°$. Regrettably, SF12 remains unsuccessful. Finally, with $B = 125$ kHz, SF7 and SF10 are successful across all angles. SF12, on the other hand, achieves success within angles below 35°, while communication fails at higher angles due to the Doppler rate.

Moving towards the 2100 MHz carrier frequency, a bandwidth B of 31.25 kHz permits communication only between 77° and 90° for SF7. On the contrary, communications for SF10 and SF12 fail throughout the entire satellite trajectory. With a $B = 62.5$ kHz, SF7 range extends to $70° < E \leq 90°$. Despite the increase in bandwidth, SF10 and SF12 could not combat the higher Doppler effect at 2.1 GHz. At a wider $B = 125$ kHz, SF7 and SF10's success range extends and it allow communication between 50° and 90°, and SF12 remains unsuccessful.

To summarize, this table offers valuable insight into the impact of carrier frequencies, bandwidths, and SFs on LoRa DtS connectivity, providing clear guidelines for successful satellite communication in different scenarios.

D. PAYLOAD

To evaluate the performance for different MAC payload lengths, we investigate the PDR. When using LPWAN $F_C = 433$ MHz band and $B = 125$ kHz, SF7 and SF10 offer 100% PDR at the maximum allowed payload lengths of 250 bytes and 59 bytes, respectively. However, as shown in Figure 8, SF12 PDR varies with the payload, and the specific behaviour depends on both F_C and B. One can see that an increase in carrier frequency and payload length worsens the PDR. Specifically, at 2.1 GHz and 125 kHz, the SF12 PDR remains zero for all payload lengths. As known, however, higher bandwidth improves reliability, and accordingly, we observe that SF12 offers PDR 80% and 100% when transmitting at $B = 250$ kHz and 500 kHz, respectively, with a payload length of 59 bytes.

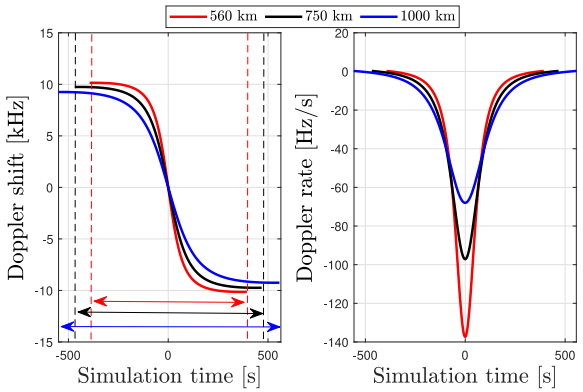

FIGURE 9. Doppler shift (left) and Doppler rate (right) as a function of the satellite orbital height at F_c = 433 MHz. The arrows indicate the satellite visibility for different orbital heights resulting in τ = [788, 935, 1113] seconds for H = [560, 750, 1000] km, respectively.

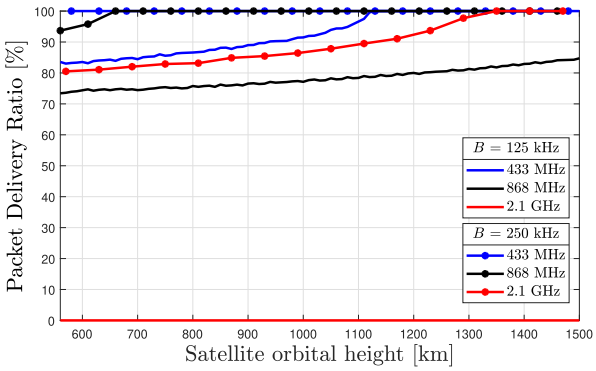

FIGURE 10. Impact of variable orbital height on SF12 PDR at B = 125 kHz, 250 kHz, F_c = 433 MHz, 868 MHz and 2.1 GHz.

E. SATELLITE ORBIT

The altitude of the satellite determines the speed required to maintain the orbit. Orbits closer to Earth require a high velocity, which reduces the visibility duration and causes a strong Doppler effect. As an example, Figure 9 shows the static and dynamic Doppler for H = [560, 750, 1000] km at F_C = 433 MHz, also highlighting the satellite visibility interval.

Figure 10, instead, plots the PDR as a function of the satellite orbital height in the case SF = 12, P_L = 59 bytes. First, we discuss the reliability of a LoRa link operating with B = 125 kHz (solid curves in Figure 10). A satellite operating at F_C = 433 MHz achieves 100% PDR at H = 1130 km. At the maximum height of 1500 km, LoRa DtS PDR for carrier frequencies of 868 MHz and 2.1 GHz remains 84% and 0%, respectively. When operating with B = 250 kHz (markers curves in Figure 10), the satellites working with F_C = 868 MHz and 2.1 GHz offer 100% PDR at 660 km and 1350 km, respectively.

VI. SUMMARY OF KEY FINDINGS AND DISCUSSION

In this manuscript, we focused on characterizing the success/failure of packet transmissions for each time-instant and elevation angle during the satellite visibility interval.

TABLE 6. The impact of key parameters on the Doppler effect in LoRa DtS connectivity.

Parameter	Static Doppler	Dynamic Doppler	Impact
SFs	×	✓	High
Payload	×	✓	Moderate
Bandwidth	✓	✓	Very high
LDRO	×	✓	Very high
Carrier frequency	✓	✓	Very high
Orbital height	✓	✓	Moderate

Figure 4 and Figure 5 are an example of such outputs. We validated our approach by comparing our results with the experimental results in the reference work [9], which were presented in the same pictorial form. In this regard, the good match between our results in Figure 4 and the flight test results (referring to Fig. 9, and [9, Table 3]) confirms the validity of our methodology and the framework proposed.

However, our investigations are more comprehensive than those presented in [9], as we explored the robustness of the LoRa modulation against the Doppler effect by considering parameters/settings that were not addressed in [9] (e.g., disabling LDRO), and by varying the configurations that were fixed in (e.g., carrier frequency, orbital height) [9].

Notably, LoRa DtS connectivity responds differently to each parameter. While changes in SF, payload length, and LDRO have no impact on the robustness against static Doppler, they do influence the vulnerability to dynamic Doppler. Conversely, variations in channel bandwidth, carrier frequency, and satellite orbital height affect both static and dynamic Doppler. A comprehensive review of the parameters that influence the robustness of LoRa modulation to the Doppler effect, along with the magnitude of their impact, is presented in Table 6.

To give an example, the PDR slightly drops by increasing the MAC payload size and decreasing the orbital height. Conversely, channel bandwidth, carrier frequency and LDRO significantly influence the performance. To ensure high reliability, one should carefully select these key parameters, also considering link budget aspects. For example, using larger bandwidths helps counteract the Doppler effect, but increases noise, thereby negatively impacting the link budget. Our results and analysis provide insights for the selection of suitable parameters and settings to mitigate the Doppler effect in the DtS link. The presented results are equally beneficial for researchers in Academia and practitioners in Industry to understand the LoRa Doppler limits for LEO satellites. For example, it can give an idea of how to select a suitable set of communication parameters, e.g., frequency band, channel bandwidth, SFs, and maximum payload for a satellite orbital height, or vice versa. Notably, in [15] we also openly-publish our codes and models to allow other scholars to facilitate understanding and reproducing the results presented in this paper. The computational complexity and the time needed to conduct the simulations mainly

depends on the parameters under investigation. For instance, with MATLAB R2023a, it takes approximately 12 seconds to produce the results depicted in Figure 4.

Finally, it is worth noting that immunity to the Doppler effect also heavily relies on designers' choices at the circuit level, and system performance can be enhanced through improvements in electronic design. To make a fair comparison with the work in [9], we considered the specifications for LoRa transceivers SX1276/77/78/79. However, LoRa transceivers (LR1120) specifically designed to operate in the presence of high Doppler shifts are expected to provide better performance in the future. Nonetheless, we are not aware of a single operational satellite using the Semtech's latest transceivers.

VII. CONCLUSION

This paper investigates the performance of LoRa DtS links considering the Doppler effect. Our results show the pros, cons and trade-offs of varying key communication and orbital parameters, i.e., SF, bandwidth, carrier frequency, LDRO, and message payload. Both the static and dynamic Doppler may disrupt the communication link resulting in packet losses. The former is particularly harmful at low elevation angles, while the latter has a greater impact at high elevation angles, when the satellite is closer to the end-device, creating a hole in the middle of the satellite footprint, thus, significantly reducing the effective coverage area. In both cases, the Doppler effect lowers the useful connection time. Consequently, even if a satellite is visible, the end-devices might not be able to communicate due to the Doppler effect. We report that bandwidth, LDRO, carrier frequency, and selection of SFs significantly impact the performance of DtS link. However, the packet payload size and satellite orbital height have a moderate influence on the performance. Our results can be useful to find a suitable set of communication parameters for a given satellite orbit to combat these packet losses. We consider the LoRa Doppler analysis accounting for the noise, attenuation and sensitivity to be a very prospective and challenging research direction for future work. More than this, we also consider it is worth investigating how LoRa modulation behaves in very low Earth orbit (VLEO). Notably, there is lack of information about the specific thresholds for static and dynamic Doppler, which requires further investigation. Finally, we consider Doppler-enabled Adaptive Data Rate, i.e., SF allocation mechanism as a promising topic for future research on LoRa DtS.

ACKNOWLEDGMENT

The authors are also thankful to Walter Ahlström foundation for supporting this work.

REFERENCES

[1] R. Marini, K. Mikhaylov, G. Pasolini, and C. Buratti, "Low-power wide-area networks: Comparison of LoRaWAN and NB-IoT performance," *IEEE Internet Things J.*, vol. 9, no. 21, pp. 21051–21063, Nov. 2022.

[2] O. Kodheli et al., "Satellite communications in the new space era: A survey and future challenges," *IEEE Commun. Surveys Tuts.*, vol. 23, no. 1, pp. 70–109, 1st Quart., 2021.

[3] M. Centenaro, C. E. Costa, F. Granelli, C. Sacchi, and L. Vangelista, "A survey on technologies, standards and open challenges in satellite IoT," *IEEE Commun. Surveys Tuts.*, vol. 23, no. 3, pp. 1693–1720, 3rd Quart., 2021.

[4] K. Mikhaylov, H. Alves, and M. Höyhtyä, "Drivers, use-cases, key indicators, and requirements for satellite-based machine type connectivity and IoT," in *Proc. 39th Int. Commun. Satell. Syst. Conf.*, 2022, pp. 221–227.

[5] G. Pasolini, "On the LoRa chirp spread spectrum modulation: Signal properties and their impact on transmitter and receiver architectures," *IEEE Trans. Wireless Commun.*, vol. 21, no. 1, pp. 357–369, Jan. 2022.

[6] A. A. Doroshkin, A. M. Zadorozhny, O. N. Kus, V. Yu. Prokopyev, and Y. M. Prokopyev, "Experimental study of LoRa modulation immunity to doppler effect in CubeSat radio communications," *IEEE Access*, vol. 7, pp. 75721–75731, 2019.

[7] M. Asad Ullah, K. Mikhaylov, and H. Alves, "Massive machine-type communication and satellite integration for remote areas," *IEEE Wireless Commun.*, vol. 28, no. 4, pp. 74–80, Aug. 2021.

[8] M. Asad Ullah et al., "Enabling mMTC in remote areas: LoRaWAN and LEO satellite integration for offshore wind farm monitoring," *IEEE Trans. Ind. Informat.*, vol. 18, no. 6, pp. 3744–3753, Jun. 2022.

[9] A. M. Zadorozhny et al., "First flight-testing of LoRa modulation in satellite radio communications in low-earth orbit," *IEEE Access*, vol. 10, pp. 100006–100023, 2022.

[10] (SEMTECH, Camarillo, CA, USA). "SX1276/77/78/79-137 MHz to 1020 MHz low power long range transceiver." (May 2020). Accessed: Jan. 5, 2023. [Online]. Available: https://www.semtech.com/products/wireless-rf/lora-connect/sx1276

[11] (SEMTECH, Camarillo, CA, USA). "Application note: LoRa® modulation crystal oscillator guidance," (Jul. 2019). Accessed: Jan. 5, 2023. [Online]. Available: https://www.semtech.com/products/wireless-rf/lora-connect/sx1276

[12] (SEMTECH, Camarillo, CA, USA). "AN1200.59 selecting the optimal reference clock," (Jul. 2022). Accessed: Jan. 5, 2023. [Online]. Available: https://www.semtech.com/products/wireless-rf/lora-connect/sx1276

[13] (SEMTECH, Camarillo, CA, USA). "SX1268 long range, low power, sub-GHz RF transceiver." (Jul. 2019). Accessed: Jan. 5, 2023. [Online]. Available: https://www.semtech.com/products/wireless-rf/lora-connect/sx1268,

[14] (SEMTECH, Camarillo, CA, USA). "AN1200.64 LR-FHSS system performance." (Feb. 2022). Accessed: Jan. 5, 2023. [Online]. Available: https://www.semtech.com/products/wireless-rf/lora-edge/lr1120

[15] M. A. Ullah. "LoRa-direct-to-satellite-the-doppler-perspectives." (2023). Accessed: Nov. 21, 2023. [Online]. Available: https://github.com/MuhammadAsadUllah1/LoRa-Direct-to-Satellite-The-Doppler-perspectives

[16] TinyGS. "TinyGS, the open source global satellite network." (2023). Accessed: Jan. 5, 2023. [Online]. Available: https://tinygs.com/satellites

[17] W. Zhou, T. Hong, X. Ding, and G. Zhang, "LoRa performance analysis for LEO satellite IoT networks," in *Proc. 13th Int. Conf. Wireless Commun. Signal Process. (WCSP)*, 2021, pp. 1–5.

[18] L. Fernandez, J. A. Ruiz-De-Azua, A. Calveras, and A. Camps, "Assessing LoRa for satellite-to-earth communications considering the impact of ionospheric scintillation," *IEEE Access*, vol. 8, pp. 165570–165582, 2020.

[19] G. Álvarez, J. A. Fraire, K. A. Hassan, S. Céspedes, and D. Pesch, "Uplink transmission policies for LoRa-based direct-to-satellite IoT," *IEEE Access*, vol. 10, pp. 72687–72701, 2022.

[20] M. A. Ullah, A. Yastrebova, K. Mikhaylov, M. Höyhtyä, and H. Alves, "Situational awareness for autonomous ships in the arctic: MMTC direct-to-satellite connectivity," *IEEE Commun. Mag.*, vol. 60, no. 6, pp. 32–38, Jun. 2022.

[21] J. Petäjäjärvi, K. Mikhaylov, M. Pettissalo, J. Janhunen, and J. H. Iinatti, "Performance of a low-power wide-area network based on LoRa technology: Doppler robustness, scalability, and coverage," *Int. J. Distrib. Sensor Netw.*, vol. 13, pp. 1–16, Mar. 2017.

[22] Y. Li, S. Han, L. Yang, F.-Y. Wang, and H. Zhang, "LoRa on the move: Performance evaluation of LoRa in V2X communications," in *Proc. IEEE Intell. Veh. Symp. (IV)*, 2018, pp. 1107–1111.
[23] A. Doroshkin, A. Zadorozhny, O. Kus, V. Prokopyev, and Y. Prokopyev, "Laboratory testing of LoRa modulation for CubeSat radio communications," in *Proc. MATEC Web Conf.*, vol. 158, 2018, p. 1008.
[24] V. Y. Prokopyev et al., "NORBY CubeSat nanosatellite: Design challenges and the first flight data," *J. Phys. Conf. Ser.*, vol. 1867, no. 1, Apr. 2021, Art. no. 12038.
[25] R. M. Colombo, A. Mahmood, E. Sisinni, P. Ferrari, and M. Gidlund, "Low-cost SDR-based tool for evaluating LoRa satellite communications," in *Proc. IEEE Int. Symp. Meas. Netw.*, 2022, pp. 1–6.
[26] G. Colavolpe, T. Foggi, M. Ricciulli, Y. Zanettini, and J.-P. Mediano-Alameda, "Reception of LoRa signals from LEO satellites," *IEEE Trans. Aerosp. Electron. Syst.*, vol. 55, no. 6, pp. 3587–3602, Dec. 2019.
[27] J. Kang, D.-H. Jung, S. Jung, J.-B. Kim, P. Kim, and J.-G. Ryu, "Regression based pilot design for doppler effect estimation and compensation in LEO satellite communication with LoRa," in *Proc. 27th Asia Pac. Conf. Commun. (APCC)*, 2022, pp. 631–632.
[28] S. Cakaj, B. Kamo, V. Koliçi, and O. Shurdi, "The range and horizon plane simulation for ground stations of low earth orbiting (LEO) satellites," *Int. J. Commun. Netw. Syst. Sci.*, vol. 4, no. 9, pp. 585–589, 2011.
[29] A. W. Doerry, "Earth curvature and atmospheric refraction effects on radar signal propagation," U.S. Dept. Energy, Sandia Nat. Lab. (SNL-NM), Albuquerque, NM, USA, Rep. SAND2012-10690, 2013.

MUHAMMAD ASAD ULLAH (Student Member, IEEE) received the master's degree in wireless communication engineering from The University of Oulu, where he is currently pursuing the Ph.D. degree in communications engineering. Since 2018, he has been with the Centre for Wireless Communications, The University of Oulu. He is a Senior Scientist with the VTT Technical Research Center of Finland Ltd., Oulu, Finland. His technical expertise include analytical and simulation modeling of wireless communications system, with a particular focus on Beyond 5G, mMTC, and non-terrestrial networks.

GIANNI PASOLINI (Member, IEEE) is an Associate Professor with the Department of Electrical, Electronic and Information Engineering, University of Bologna, where he has been teaching various courses in the field of telecommunications since 2003. His research interests encompass wireless communication systems, Internet of Things, digital signal processing, and THz communications. Throughout his career, he has actively participated in several European initiatives focused on wireless communications, including COST actions and Networks of Excellence. He serves as an Associate Editor for the IEEE OPEN JOURNAL OF THE COMMUNICATIONS SOCIETY. He served as a member of the organizing committee for several IEEE conferences. He is one of the founding members of the "National Laboratory of Wireless Communications - Wilab" of the National Inter-University Consortium for Telecommunications, Italy.

KONSTANTIN MIKHAYLOV (Senior Member, IEEE) is an Assistant Professor for Convergent IoT Communications for Vertical Systems with the Centre for Wireless Communications, The University of Oulu. He has authored or coauthored about one hundred research contributions on wireless connectivity for IoT, system design, and applications. His research focuses on radio access and beyond-access technologies for massive and dependable IoT and the matters related to the design and performance of IoT devices and systems.

HIRLEY ALVES (Member, IEEE) is currently an Associate Professor and the Head of the Machine-Type Wireless Communications Group, 6G Flagship, Centre for Wireless Communications, The University of Oulu. He actively works on massive connectivity and ultra-reliable low latency communications for future wireless networks, 5GB and 6G, full-duplex communications, and physical-layer security. In addition, he leads the URLLC activities for the 6G Flagship Program. He has received several awards and has been an organizer, the chair, a TPC, and a tutorial lecturer for several renowned international conferences. He is the General Chair of the ISWCS 2019 and the General Co-Chair of the First 6G Summit, Levi 2019, and ISWCS 2021.